J Therm Anal Calorim (2014) 117:1047–1063
DOI 10.1007/s10973-014-3892-2

Thermal and dielectric properties of newly developed linear aliphatic-ether linked bismaleimide-polyhedral oligomeric silsesquioxane (POSS-AEBMI) nanocomposites

S. Devaraju · M. R. Vengatesan · M. Selvi · M. Alagar

Received: 19 July 2013 / Accepted: 25 May 2014 / Published online: 24 July 2014

Abstract A new series of four different linear aliphatic ether linked aromatic bismaleimides (AEBMIs) were synthesized from the respective linear aliphatic ether-linked aromatic diamines and maleic anhydride. Further, the POSS-AEBMI nanocomposites were developed by Michael addition reaction of bismaleimide with varying mass percentages of octa(aminophenyl)silsesquioxane and were characterized by the fourier transform infrared spectroscopy, differential scanning calorimetry, and thermogravimetric analysis. Data from thermal studies revealed that the POSS-reinforced AEBMI nanocomposites possesses higher glass transition temperature (*Tg*), thermal stability, limiting oxygen index, and lower dielectric constant when compare to that of neat AEBMI. X-ray diffraction and transmission electron microscopy analysis confirmed the molecular level dispersion of POSS in the AEBMI matrix.

Keywords Bismaleimide · POSS · Thermal properties · Flame retardant · Dielectric properties · Nanocomposites

S. Devaraju · M. R. Vengatesan · M. Selvi · M. Alagar (✉)
Polymer Nanocomposite Lab, Department of Chemical Engineering, Anna University, Chennai 600 025, India
e-mail: mkalagar@yahoo.com

S. Devaraju
Next MEMS Lab, School of Mechanical Engineering, Pusan National University, Busan 609-735, South Korea

M. R. Vengatesan
School of Electronic and Electrical Engineering, Sungkyunkwan University, Suwon, South Korea

Introduction

Organic–inorganic hybrids with covalent bonding between organic and inorganic components at the molecular level are widely regarded as one of the most promising and rapidly emerging materials. The properties of organic–inorganic hybrid materials obtained from the polymeric and inorganic components provide an easy processability, better toughness, and good thermal and oxidative stability [1–6].

Recently, a novel class of organic–inorganic hybrid materials based on polyhedral oligomeric silsesquioxane (POSS) has been developed. POSS has the advantages of having monodisperse molecular mass, with a well-defined structure, lower density, high-temperature stability, and containing no trace metals, and sizable interfacial interaction between composite particles and polymer segments. Each POSS compound may contain one or more reactive sites; therefore, it can be easily incorporated into common polymers. To improve the property of the material, POSS can be introduced into the matrix with polymerizable groups [7–20]. In our earlier work, POSS-polyimide, POSS-polybenzoxazine, and POSS-epoxy nanocomposites have been studied; and the data from the different analyses revealed significant improvements in thermal and low dielectric properties [21–28].

Bismaleimide (BMI) resins are one of the important advanced resin matrices used for composites, and play an increasingly important role in high-tech applications due to the fact that their cured products have good electrical properties, lower coefficients of thermal expansion, excellent fire and moisture resistance, superior thermal and thermo-oxidative stability, higher glass transition temperatures, and better mechanical strength [29–32]. However, their inherent brittleness and limited impact resistance, resulting from high crosslink density and rigid molecular

Scheme 1 Synthesis of linear aliphatic ether-linked aromatic bismaleimide ($AEBMI_{1–4}$)

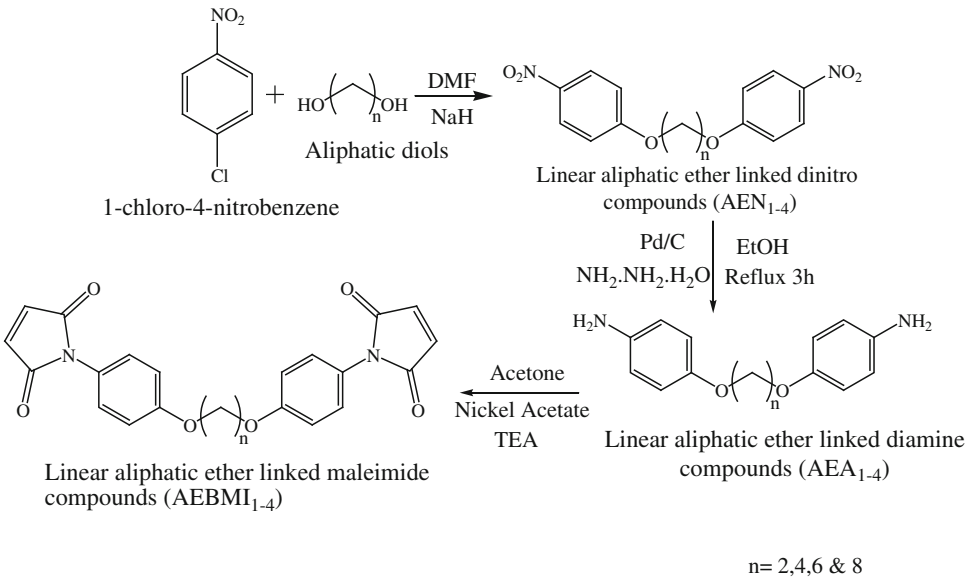

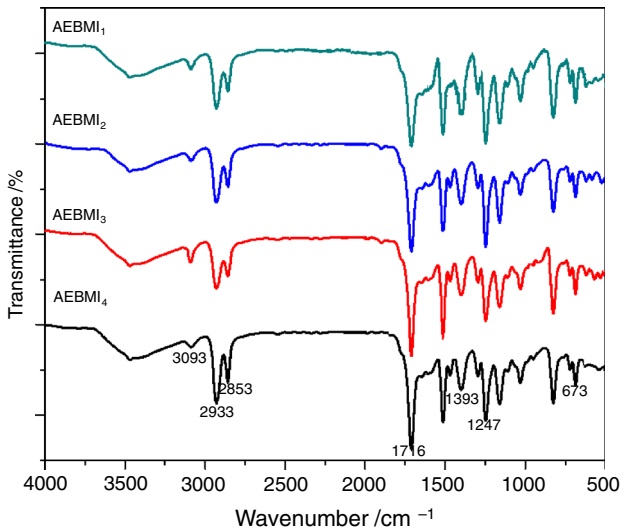

Fig. 1 FT-IR Spectra of linear aliphatic ether-linked bismaleimide ($AEBMI_{1–4}$)

skeleton, hamper their further application in aerospace and electronic industries. Hence, many modification methods have been developed to overcome the above-mentioned drawbacks. Chemical modifications, such as the incorporation of flexible ether linkage on the main chain and/or introduction of a bulky pendant group on the diamine, help in producing a wide range of BMI with improved utility. The presence of flexible ether linkage would decrease the rigidity and crystallinity lower the energy of the internal rotation of the polymer chain and enhance the solubility. The incorporation of a bulky pendant group is expected to decrease the close packing of polymer chains, which decreases the intermolecular forces of attraction, thereby improving the processability of the polymer [33–35].

In the present work, a new type of POSS-AEBMI hybrid composite materials were developed from linear aliphatic ether-linked diamine-based BMI with the incorporation of varying mass percentages (1, 3, and 5 mass%) of octa(aminophenyl)silsesquioxane (OAPS) through the Michael addition reaction and were characterized using the fourier transform infrared spectroscopy (FT-IR), differential scanning calorimetry (DSC) and thermogravimetric analysis (TG) techniques. It was observed that the resulting OAPS reinforced-AEBMI exhibits higher thermal and dielectric properties than those of neat AEBMI.

Experimental procedure

Materials

Maleic anhydride, 1,2-ethenediol, 1,4-butanediol, 1,6-hexanediol, and 1,8-octanediol were received from TCI chemicals Ltd. Sodium hydride, 1-chloro-4-nitrobenzene, formaldehyde (37%), and phenol were received from LOBA chemicals. All the solvents were received from SRL India Ltd. All the chemicals were used without any further purification. OAPS (Scheme 1) was synthesized and characterized as per reported procedure [21, 22].

Synthesis of linear aliphatic ether-linked aromatic dinitro compounds ($AEN_{1–4}$)

100 mL of dry dimethylformamide (DMF), sodium hydride, and 10 g (0.1611 mol) of 1,2- ethanediol were

taken in a 250-mL round-bottomed flask. The resultant product was stirred for 3 h at 50 °C and cooled to 0–5 °C to get the sodium salt of diol. Then, 50.7 g (0.3222 mol) of 1-chloro-4-nitrobenzene was dissolved in 100 mL of DMF. This was slowly added to the sodium salt of diol at the same temperature, and then the temperature was raised to 30 °C and stirred over night. The reaction mass was quenched with 1,500 g of crushed ice, filtered and washed with distilled water, and recrystallized with ethanol. Yield: 91 % (Scheme 1). $AEN_{2–4}$ was synthesized as per the above procedure using respective diols and 1-chloro-4-nitrobenzene.

Synthesis of linear aliphatic ether-linked aromatic diamine compound ($AEA_{1–4}$)

100 mL of ethanol, 10 g of aliphatic ether-linked nitro compound AEN_1, and 1 g of 10 % Pd/C were taken in a 250-mL round-bottomed flask. The temperature of the mixture was raised to 50 °C, and then 20 mL of hydrazine hydrate was added to the mixture and refluxed for 3 h. The content was filtered in hot condition and cooled to room temperature, to get white crystals. Yield: 86 % (Scheme 1). $AEA_{2–4}$ was synthesized by the reduction of respective dinitro compounds.

AEA_1: FT-IR: 3397 (–NH_2), 2927 (Symmetric stretching), 2862 (asymmetric stretching), 1594 (Ar stretching), 1227 (Ar–O–CH_2).

^{1}H NMR (500 MHz, $CDCl_3$) δ (ppm): 6.52 (d, 4H, ArH), 6.37 (d, 4H, ArH), 4.36 (t, 4H, Ar–O–CH_2).

^{13}C NMR: 147,140,116,115 (aromatic carbon), 69 (aliphatic carbon).

AEA_2: FT-IR: 3391 (–NH_2), 2922 (Symmetric stretching), 2860 (asymmetric stretching), 1594 (Ar stretching), 1221 (Ar–O–CH_2).

^{1}H NMR (500 MHz, $CDCl_3$) δ (ppm): 6.61 (d, 4H, ArH), 6.42 (d, 4H, ArH), 4.41 (t, 4H, Ar–O–CH_2), 3.91 (t, 4H, –O–CH_2–CH_2–) 1.82 (t, 4H, –CH_2–CH_2).

^{13}C NMR: 146,142,117,114 (aromatic carbon), 69, 26 (aliphatic carbon).

AEA_3: FT-IR: 3386 (–NH_2), 2920 (Symmetric stretching), 2836 (asymmetric stretching), 1586 (Ar stretching), 1232 (Ar–O–CH_2).

^{1}H NMR (500 MHz, $CDCl_3$) δ (ppm): 6.71 (d, 4H, ArH), 6.53 (d, 4H, ArH), 4.46 (t, 4H, Ar–O–CH_2), 3.87 (t, 4H, –O–CH_2–CH_2–) 1.78 (t, 4H, –CH_2–CH_2), 1.4 (t, 4H, –CH_2–CH_2–).

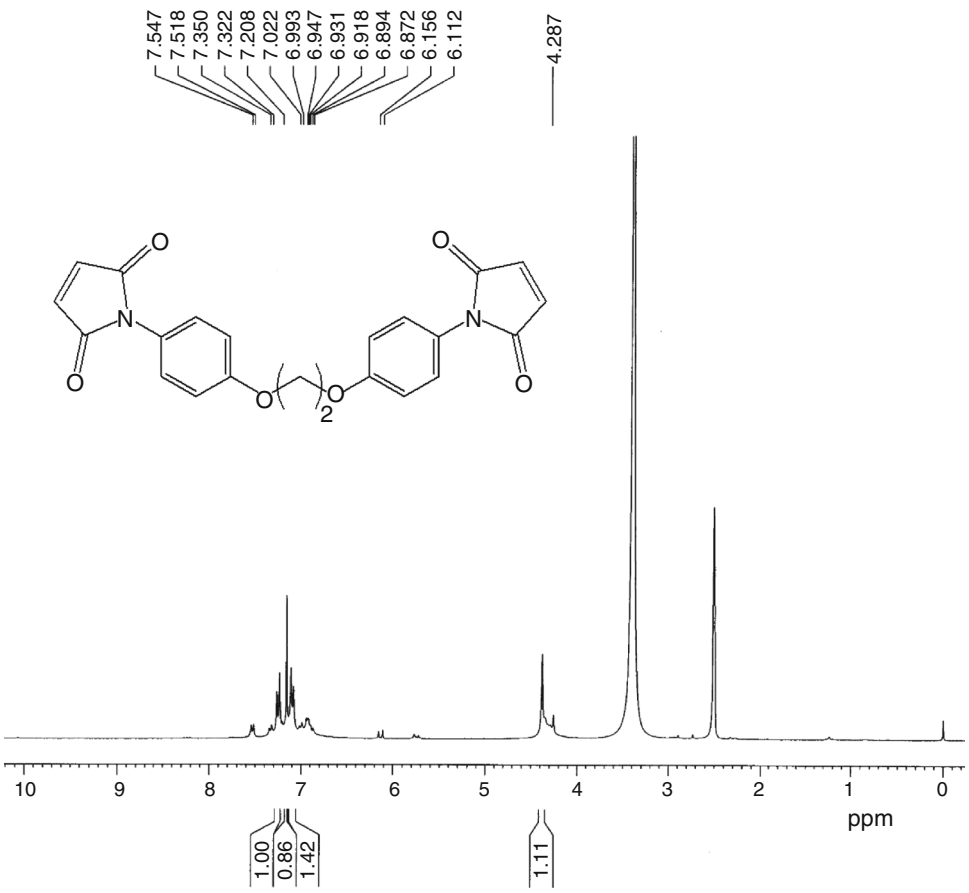

Fig. 2 ^{1}H NMR Spectrum of 1,2-bis (4-maleimidophenoxy)ethane ($AEBMI_1$)

^{13}C NMR: 146,142,117,114 (aromatic carbon), 69, 31, 25 (aliphatic carbon).

AEA_4: FT-IR: 3378 ($–NH_2$), 2932 (symmetric stretching), 2857 (asymmetric stretching), 1582 (Ar stretching), 1237 ($Ar–O–CH_2$).

^{1}H NMR (500 MHz, $CDCl_3$) δ (ppm): 6.77 (d, 4H, ArH), 6.63 (d, 4H, ArH), 4.49 (t, 4H, $Ar–O–CH_2$), 3.83 (t, 4H, $–O–CH_2–CH_2–$) 1.72 (t, 4H, $–CH_2–CH_2$), 1.35–1.42 (t, 8H, $–CH_2–CH_2–CH_2–CH_2–$).

^{13}C NMR: 146,142,117,114 (aromatic carbon), 69, 32, 27 (aliphatic carbon).

Synthesis of linear aliphatic ether-linked aromatic BMI compound ($AEBMI_{1-4}$)

To a one-Liter three-necked round-bottom flask fitted with paddle stirrer, reflux condenser, and nitrogen inlet, 600 mL acetone, 98.1 g (1.0 mol) maleic anhydride, and 0.5 mol of the AEA_1 were added. Rapid formation of precipitate of the bismaleiamic acid occurred on mixing the reactants together, and the mixture was allowed to stand for 30 min to complete the reaction [36]. To the above, 1.0 g of nickel acetate and 25 mL of triethylamine were added and the entire mixture was heated slowly to reflux. Then by means of pressure equalizing funnel, 118 mL acetic anhydride was added to the refluxing reaction mixture, and heating was continued for an additional 3 h. The reaction mixture was diluted with 500 mL water and chilled to crystallize the BMI. Yield 92 % (Scheme 1). $AEBMI_{2–4}$ was synthesized as per the above procedure using respective amines.

$AEBMI_1$: FT-IR: 3093 (C=C), 2933 (Symmetric stretching), 2853 (asymmetric stretching), 1716 (C=O stretching), 1393 (C–N–C stretching), 1247 ($Ar–O–CH_2$), 673 (C=C).

^{1}H NMR: (300 MHz, DMSOd^6) δ (ppm): 7.5–7.2 (d, 4H, ArH), 6.9–6.8 (d, 4H, ArH), 6.1 (s, 4H, CH=CH), 4.28 (t, 4H, $Ar–O–CH_2$).

^{13}C NMR: 170,157,134,128, 123, 114 (aromatic carbon), 66 (aliphatic carbon).

$AEBMI_2$: FT-IR: 3093 (C=C), 2935 (Symmetric stretching), 2854 (asymmetric stretching), 1718 (C=O stretching), 1393 (C–N–C stretching), 1247 ($Ar–O–CH_2$), 673 (C=C).

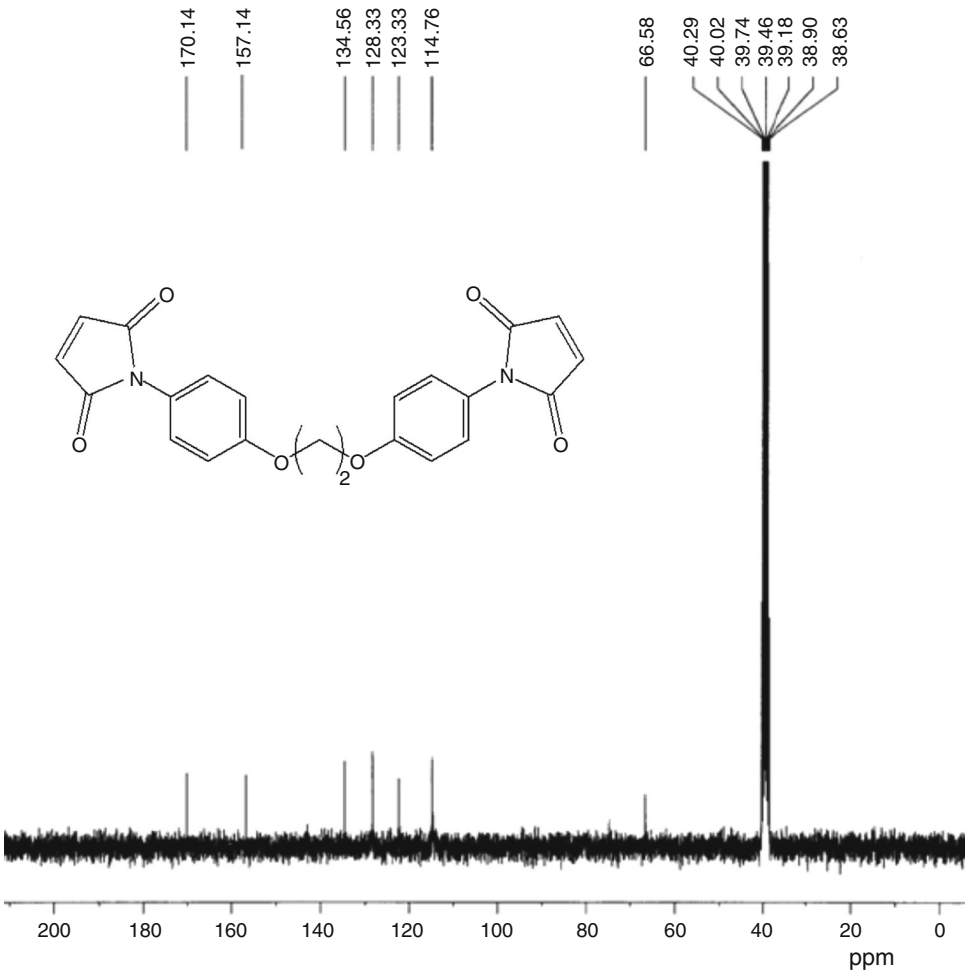

Fig. 3 ^{13}C NMR Spectrum of 1,2-bis (4-maleimidophenoxy)ethane ($AEBMI_1$)

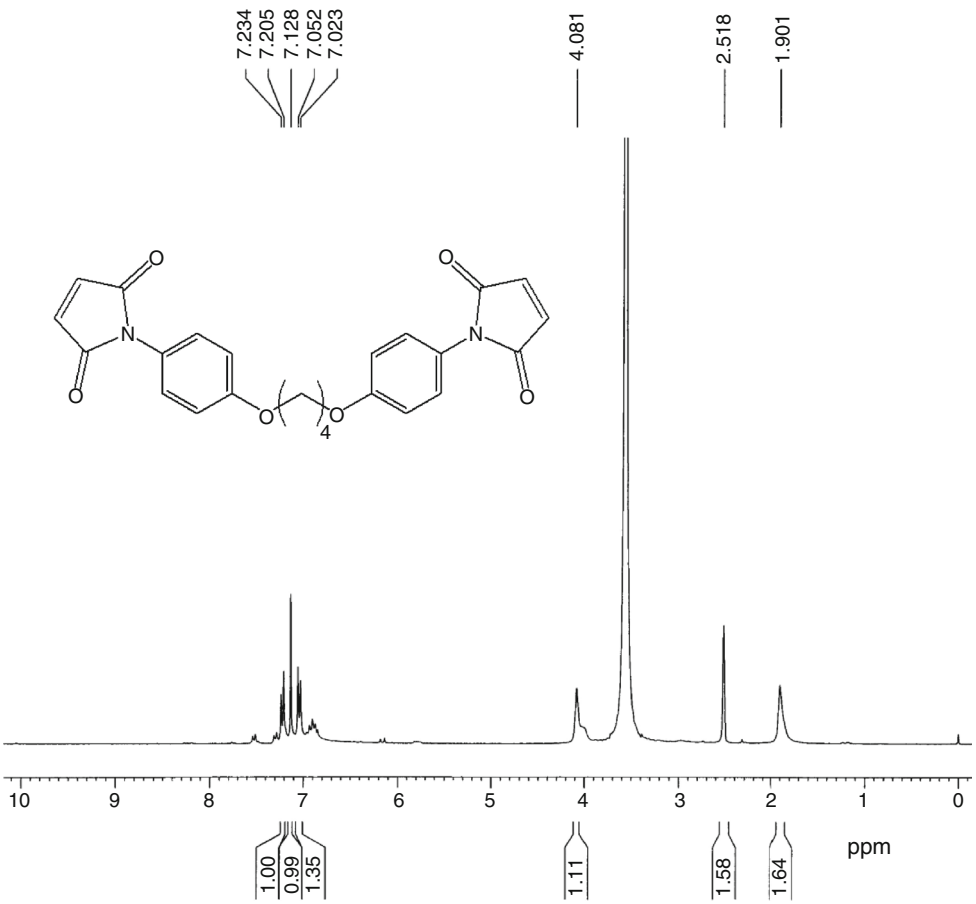

Fig. 4 ^{1}H NMR Spectrum of 1,4-bis (4-maleimidophenoxy)butane ($AEBMI_2$)

^{1}H NMR: (300 MHz, DMSOd^{6}) δ (ppm): 7.2 (d, 4H, ArH), 7.1 (d, 4H, ArH), 7.0 (S, 4H, CH=CH), 4.1 (t, 4H, Ar–O–CH_2), 1.9 (t, 4H,–CH_2–CH_2).

^{13}C NMR: 170,158,134,128,124,115 (aromatic carbon), 67, 25 (aliphatic carbon).

$AEBMI_3$: FT-IR: 3093 (C=C), 2934 (Symmetric stretching), 2854 (asymmetric stretching), 1717 (C=O stretching), 1393 (C–N–C stretching), 1247 (Ar–O–CH_2), 673 (C=C).

^{1}H NMR: (300 MHz, DMSOd^{6}) δ (ppm): 7.5 (d, 4H, ArH), 7.2–6.8 (d, 4H, ArH), 6.1 (t, 4H, CH=CH), 4.0–3.9 (t, 4H, Ar–O–CH_2), 1.8 (t, 4H, –CH_2–CH_2), 1.5 (t, 4H, –CH_2–CH_2–).

^{13}C NMR: 170,158,134,128,123,114 (aromatic carbon), 67, 28, 25 (aliphatic carbon).

$AEBMI_4$: FT-IR: 3093 (C=C) 2935 (Symmetric stretching), 2854 (asymmetric stretching), 1718 (C=O stretching), 1393 (C–N–C stretching), 1247 (Ar–O–CH_2), 673 (C=C).

^{1}H NMR: (500 MHz, DMSO d^{6}) δ (ppm): 7.1 (d, 4H, ArH), 7.0 (d, 4H, ArH), 6.9 (t, 4H, CH=CH), 3.9 (t, 4H, Ar–O–CH_2), 1.6 (t, 4H, –CH_2–CH_2), 1.3 (t, 8H, –CH_2–CH_2–).

^{13}C NMR: 170,158,135,128,124,115 (aromatic carbon), 68, 29, 25 (aliphatic carbon).

Preparation of POSS-AEBMI nanocomposites

The POSS-AEBMI nanocomposites were developed via the Michael addition reaction between OAPS and AEBMI using DMF as a solvent in an inert atmosphere. Known quantities of AEBMI and varying mass ratios of OAPS (1, 3, and 5 mass%) were dissolved in DMF. The resulting solutions were mixed in a two-necked round-bottomed flask that had been purged with nitrogen to remove moisture. The reactants were stirred under nitrogen at 100 °C for 1 h, and then cast on a smooth glass substrate and thermally treated at 100 °C for 2 h, 140 °C for 2 h, and 180 °C for 2 h.

Characterizations

FT-IR spectra were recorded on a Perkin Elmer 6X FT-IR spectrometer. About 100 mg of optical-grade KBr was ground with sufficient quantity of the solid sample to make 1 mass% mixture for making KBr pellets. All ^{1}H NMR and ^{13}C NMR analyses were done in DMSO d^{6} and recorded on a Bruker 500 spectrometer.

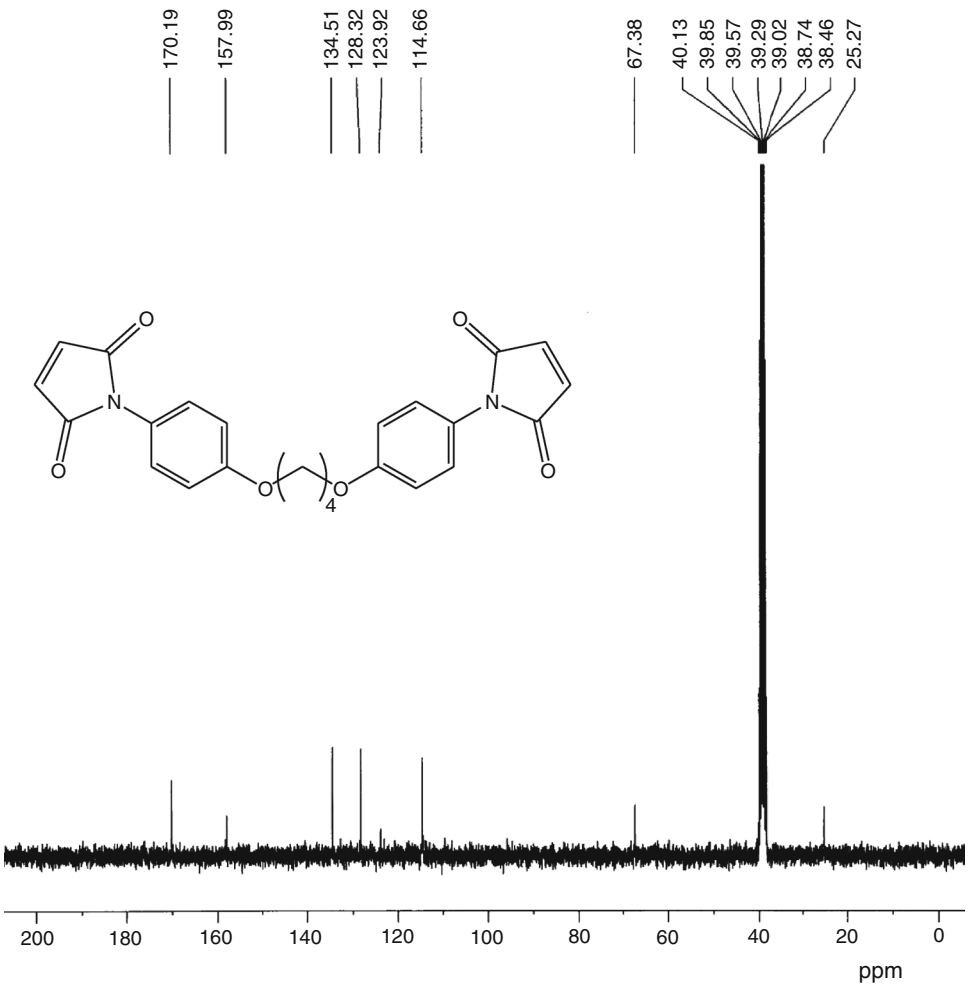

Fig. 5 ^{13}C NMR Spectrum of 1,4-bis (4-maleimidophenoxy)butane ($AEBMI_2$)

The calorimetric analysis was performed on a Netzsch DSC-200 differential scanning calorimeter. The instrument was calibrated with Indium supplied by Netzsch. Measurements were performed under a continuous flow of nitrogen (20 mL min^{-1}). All the samples (about 10 mg) were heated from ambient temperature to 300 °C, and the curves were recorded at a heating rate of 5 °C min^{-1}. Thermogravimetric analysis (TG) was performed on a Netzsch STA 409 thermogravimetric analyzer. The instrument was calibrated with calcium oxalate and aluminum supplied by Netzsch. The samples (about 10 mg) were heated from ambient temperature to 700 °C under a continuous flow of nitrogen (20 mL min^{-1}), at 10 °C min^{-1}.

The dielectric constant of the neat AEBMI and the POSS-modified AEBMI systems were determined with the help of impedance analyzer (Solartron impedance/gain phase analyzer 1260) at room temperature using platinum (Pt) electrode at a frequency range of 1 MHz. This experiment was repeated four times at the same conditions.

Wide-angle X-ray diffraction (XRD) was obtained using a Rich Seifert (Model 3000) diffractometer (with Cu $K_{\propto}$ radiation ($\theta = 0.15418$ nm) for the ground powder of the cured composites. The spectral window ranges from $2\theta = 1°$ to $2\theta = 70°$.

A JEOL JEM-3010 analytical transmission electron microscope, operating at 300 kV with a measured point-to-point resolution of 0.23 nm, was used to characterize the phase morphology of the POSS-modified AEBMI systems. The transmission electron microscopy (TEM) samples were prepared by dissolving the polymers in DMF mounted on carbon-coated Cu TEM grids and dried for 24 h at room temperature (RT) to form a film.

Results and discussion

Bismaleimide monomers were synthesized according to the routes shown in Scheme 1. All the monomers were

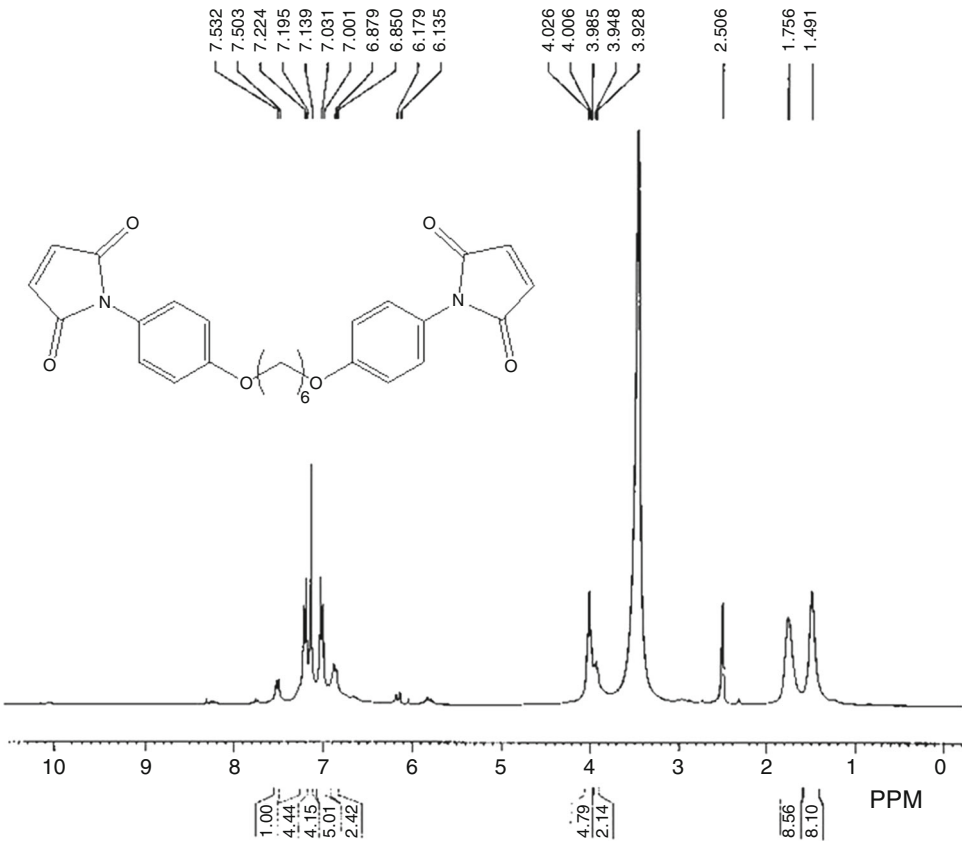

Fig. 6 ^{1}H NMR Spectrum of 1,6-bis (4-maleimidophenoxy)hexane ($AEBMI_3$)

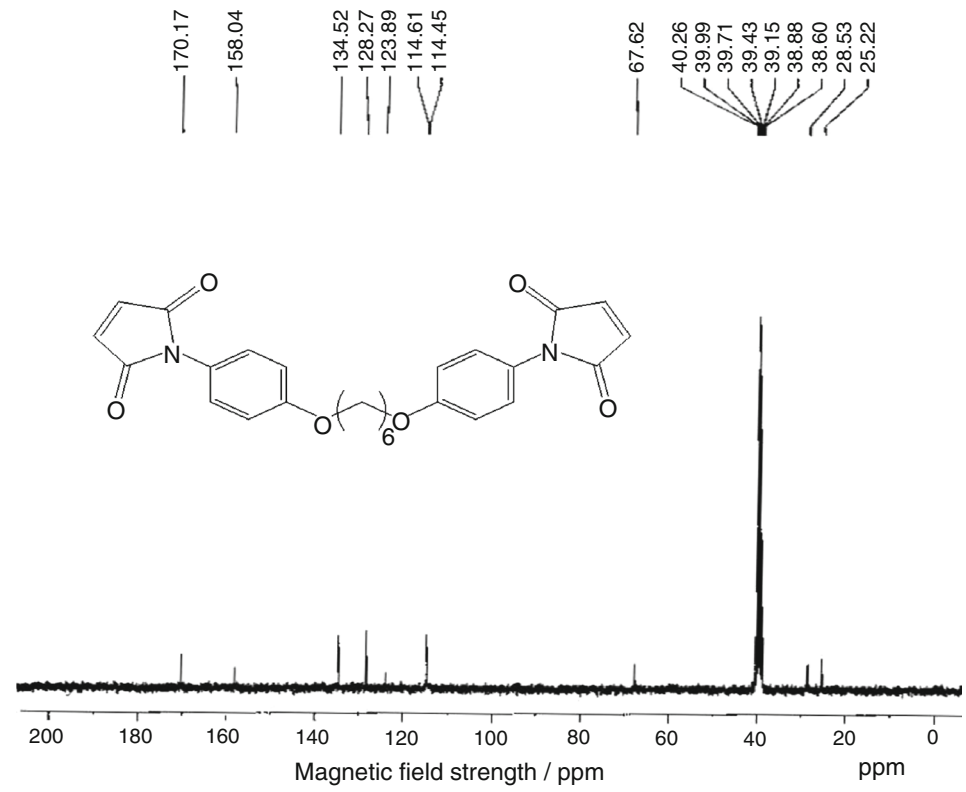

Fig. 7 ^{13}C NMR Spectrum of 1,6-bis (4-maleimidophenoxy)hexane ($AEBMI_3$)

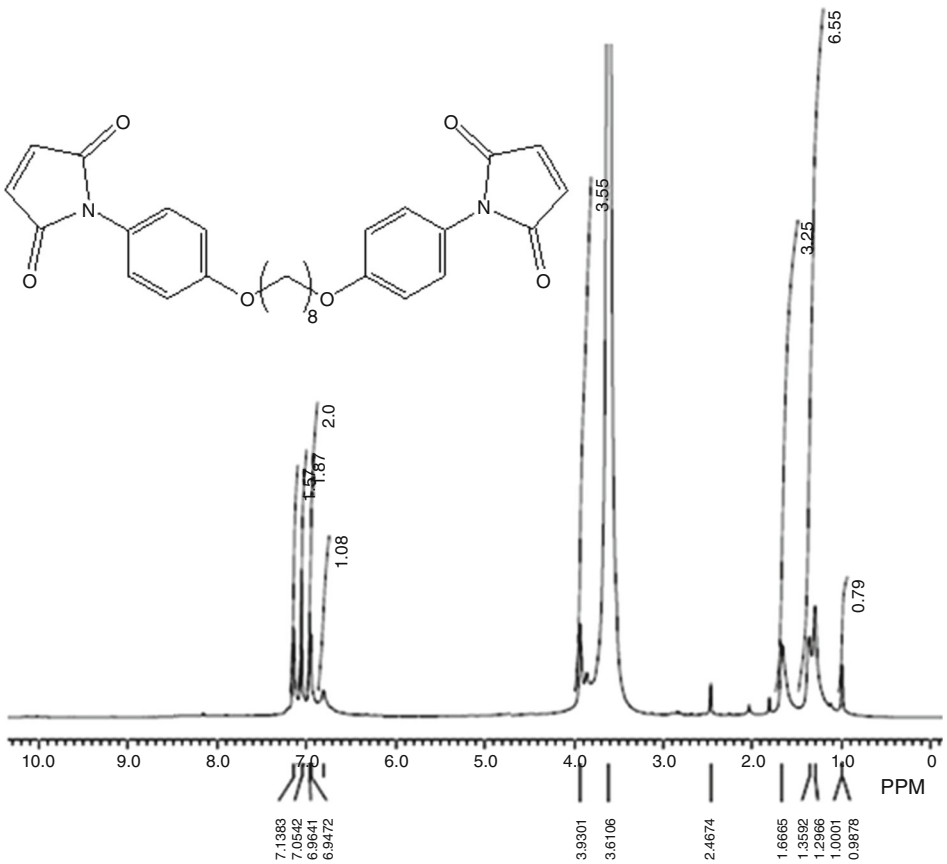

Fig. 8 ^{1}H NMR Spectrum of 1,8-bis (4-maleimidophenoxy)octane ($AEBMI_4$)

analyzed by the FTIR and NMR analyses to confirm their molecular structure. Figure 1 shows the FT-IR spectra of AEBMI monomers; the peaks appeared at about 666 and 3,110 cm^{-1} confirm the presence of C=C in BMI; also the strong absorption around 1,720 cm^{-1} confirms C=O stretching vibration of the imide ring. The bands around 1,355 cm^{-1} are due to C–N–C stretching vibration of the imide ring. Figures 2–9 show the NMR spectra of aliphatic ether-linked aromatic BMIs (AEBMIs) which further confirmed the molecular structures of AEBMIs.

The POSS-AEBMI nanocomposites were developed through the reaction of varying mass percentages (1, 3, and 5 mass%) of OAPS with AEBMI monomers via the Michael addition reaction (Scheme 2). The cured POSS-AEBMI hybrid nanocomposites were examined by the FTIR and are shown in Fig. 10. The characteristic absorption peak appeared at 1,148 cm^{-1} and associated with the maleimide C–N–C groups of AEBMI disappeared, whereas the absorption band around 1,181 cm^{-1}, corresponding to the C–N–C groups of the maleimide appeared. At the same time, the intensity of the absorption bands that appeared at 830 and 690 cm^{-1} is due to C=C and C=C–H, respectively. This indicated the occurrence of the addition reaction of the C=C of maleimide groups. The performance of the Michael addition reaction was confirmed by the absence of the bands at about 666 and 3,110 cm^{-1}. The absorption peaks appeared at 1,720 cm^{-1} for C=O stretching of the imide group, and at 1,630 cm^{-1} for the -NH group, and a peak at 3,471 cm^{-1} due to the secondary -NH stretching confirmed the occurrence of the Michael addition reaction between OAPS and AEBMI.

The glass transition temperatures (*Tg*) of the neat AEBMI, 1, 3, and 5 mass% OAPS-incorporated AEBMI systems, were studied, using the DSC analysis with the

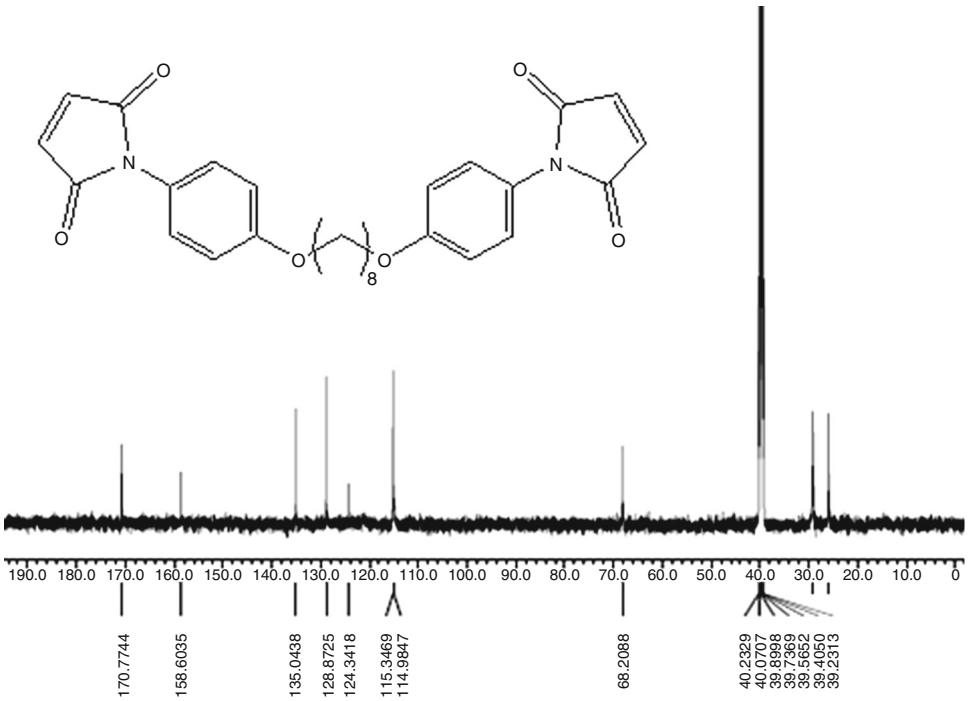

Fig. 9 ^{13}C NMR Spectrum of 1,8-bis (4-maleimidophenoxy)octane ($AEBMI_4$)

temperature ranging from ambient temperature to 300 °C at the heating rate of 5 °C min^{-1}. The DSC data obtained for the cured neat AEBMI and OAPS-incorporated AEBMI hybrid systems are presented in Fig. 11 and Table 1. The data from the DSC analysis show that the OAPS-incorporated AEBMI system possesses higher values of *Tg* than that of neat AEBMI. There are two factors that influence the glass transition temperature (*Tg*) value of the resulting materials [28]. The first factor, the hindering effect of POSS cubes on polymer chain motions enhances the values of *Tg*. The second factor, the increase in the free volume of the system due to the inclusion of bulky POSS cubes decreases the values of *Tg*. Therefore, the glass transition temperature of the POSS-containing nanocomposites would be a comprehensive result of these two factors. Although the incorporation of POSS increases the free volume in the OAPS-AEBMI nanocomposites, this effect can be compensated by an increase in the cross-linking density. Similar results were observed with POSS-PI and POSS-PBZ systems [21–26]. From the series of systems studied, the values of *Tg* decrease with an increase in the chain length of AEBMI, due to the increased free rotational movement caused by the presence of flexible linear ether linkage between the two aspartimide units.

The thermal properties of neat AEBMI and 1, 3, and 5 mass% OAPS-incorporated AEBMI systems were studied using the TG analysis with temperatures ranging from ambient temperature to 700 °C at the heating rate of 10 °C min^{-1} for nitrogen and air atmosphere. Figures 12 and 13 and Table 1 show the thermal degradation of neat AEBMI and 1, 3, and 5 mass% OAPS-incorporated BMI hybrid nanocomposites. From the TG data, it is inferred that the increasing percentages incorporation of OAPS into the AEBMI systems increased the thermal stability due to the formation of a strong covalent bond between the OAPS and AEBMI. When the OAPS content was increased, more number of imide linkages was formed, and the OAPS become an integral part of the AEBMI systems. A similar trend was observed and the values of higher char yield were obtained due to the thermally

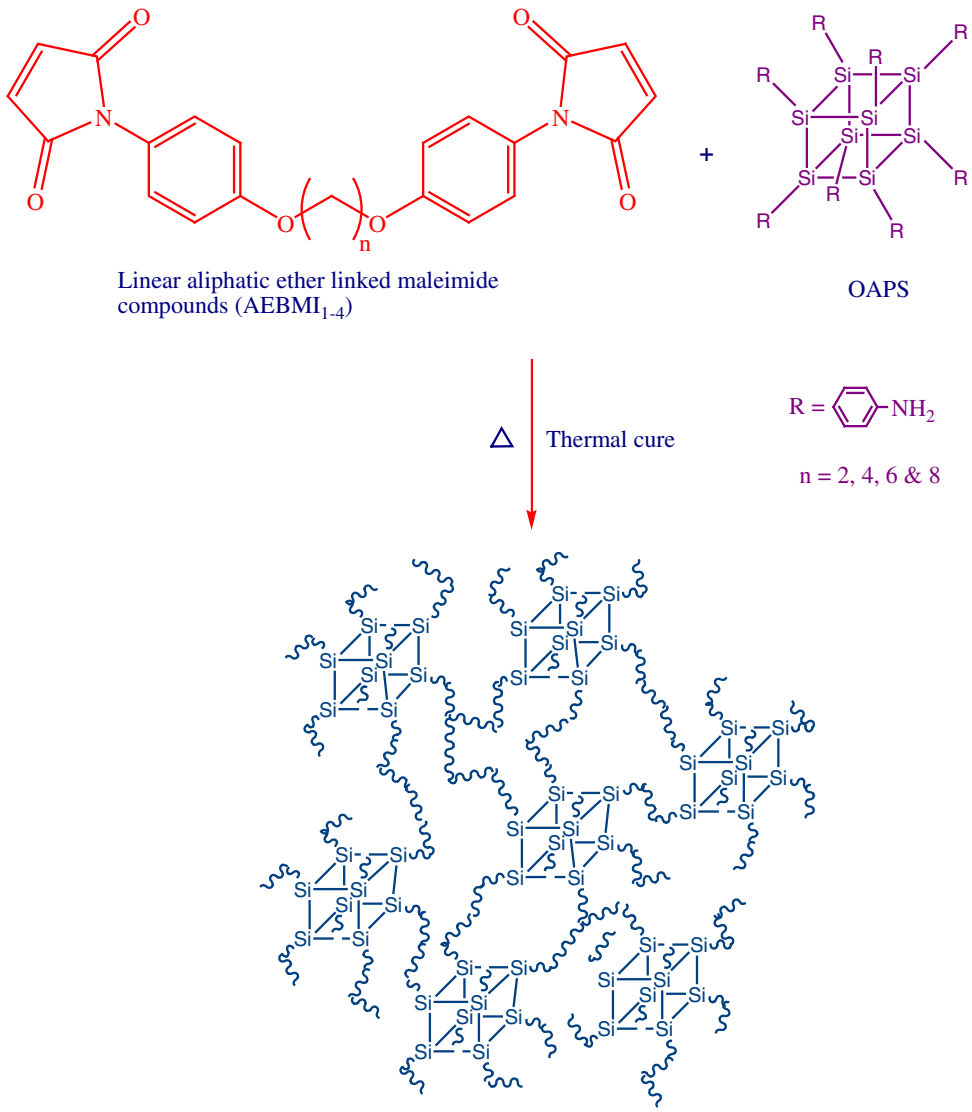

Scheme 2 Schematic representation of OAPS-incorporated AEBMI nanocomposites

stable POSS cube. Among the systems studied ($AEBMI_{1–4}$) the 1 % OAPS-incorporated $AEBMI_1$ system possesses lower initial degradation temperature when compared to other systems, and the OAPS-incorporated $AEBMI_1$ system possesses the highest thermal stability, and the OAPS-incorporated $AEBMI_4$ shows the lowest thermal stability; the other two systems ($AEBMI_2$ and $AEBMI_3$) lie between these two limits; this is due to the aliphatic chain present in the system, which induces the free rotational movement.

The limiting oxygen index (LOI) of neat AEBMI and OAPS-reinforced AEBMI hybrid systems are presented in Fig. 14 and Table 1. They are used to assess and quantify the flame-retardant behavior of polymers. The value of LOI is calculated from the char yield resulting from the TG analysis. The data obtained from the TG analysis indicate that there is an increase in the char residue as the incorporation of OAPS is increased. The LOI value represents the minimum requirement of oxygen in a nitrogen–oxygen (air) mixture, to maintain the combustion of a material (van Krevelen). The correlation between the char yield and the LOI value is represented by Eq. 1

$$\mathrm{LOI} = 17.5 + 0.4\,\sigma \tag{1}$$

where 'σ' is the char yield obtained at 700 °C.

The LOI value of OAPS-incorporated POSS-AEBMI hybrid systems is higher than that of the neat AEBMI matrix. The significant increase in the value of LOI indicates that the OAPS-reinforced AEBMI nanocomposites exhibit better flame retardancy than that of neat BMI matrix. Among the systems, the $AEBMI_1$-based POSS-AEBMI system exhibited better flame retardancy when compared to those of other systems.

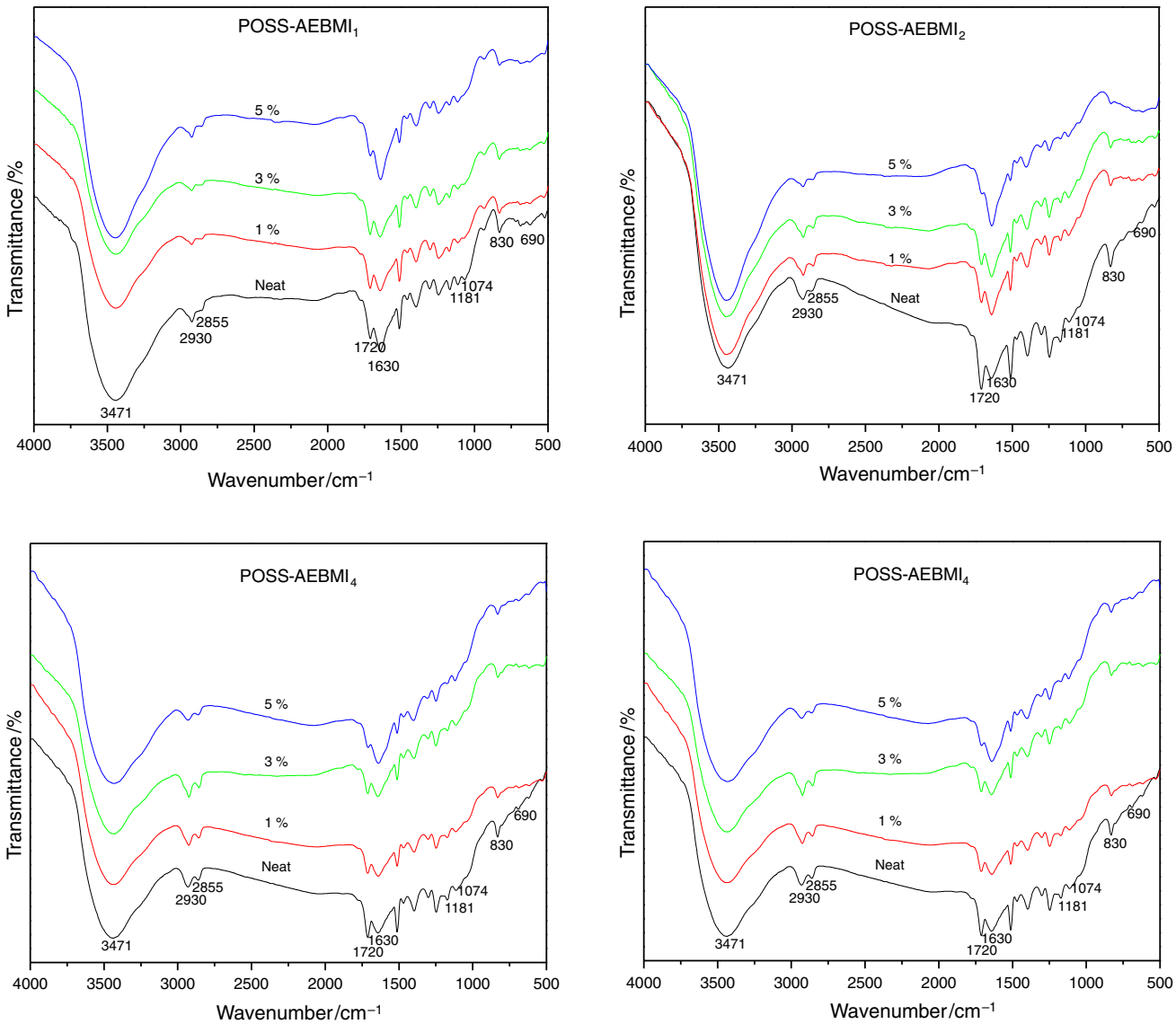

Fig. 10 FTIR Spectra of POSS-AEBMI nanocomposites

The dielectric constants ($\acute{\varepsilon}$) and dielectric loss and dielectric loss ($''\varepsilon$) of neat AEBMIs and POSS-AEBMI hybrid nanocomposites were measured, using the impedance analyzer at a frequency of 1 MHz. The value of the dielectric constant ($\acute{\varepsilon}$) and dielectric loss ($''\varepsilon$) was based mainly on the polarizability of a material, and the $\acute{\varepsilon}$ and $''\varepsilon$ value could be lowered significantly with the incorporation of less polarizable components. As shown in Fig. 15 and Table 1, the incorporation of the nanoporous OAPS molecule into the AEBMI decreased the values of the dielectric constant of the resulting POSS-AEBMI nanocomposites. The decreasing trend of dielectric properties as the increase of POSS loadings in the hybrids suggests that the increasing of POSS loading decreases the dipole–dipole interactions in the nanocomposites. The dielectric loss values of OAPS-reinforced AEBMI nanocomposites lie in between 0.004 and 0.005. By the introduction of OAPS into AEBMI systems, the dielectric constant values are reduced, and the dielectric loss was slightly decreased due to the change in free volume and the presence of less polar nature of OAPS in the resulting nanocomposites. The

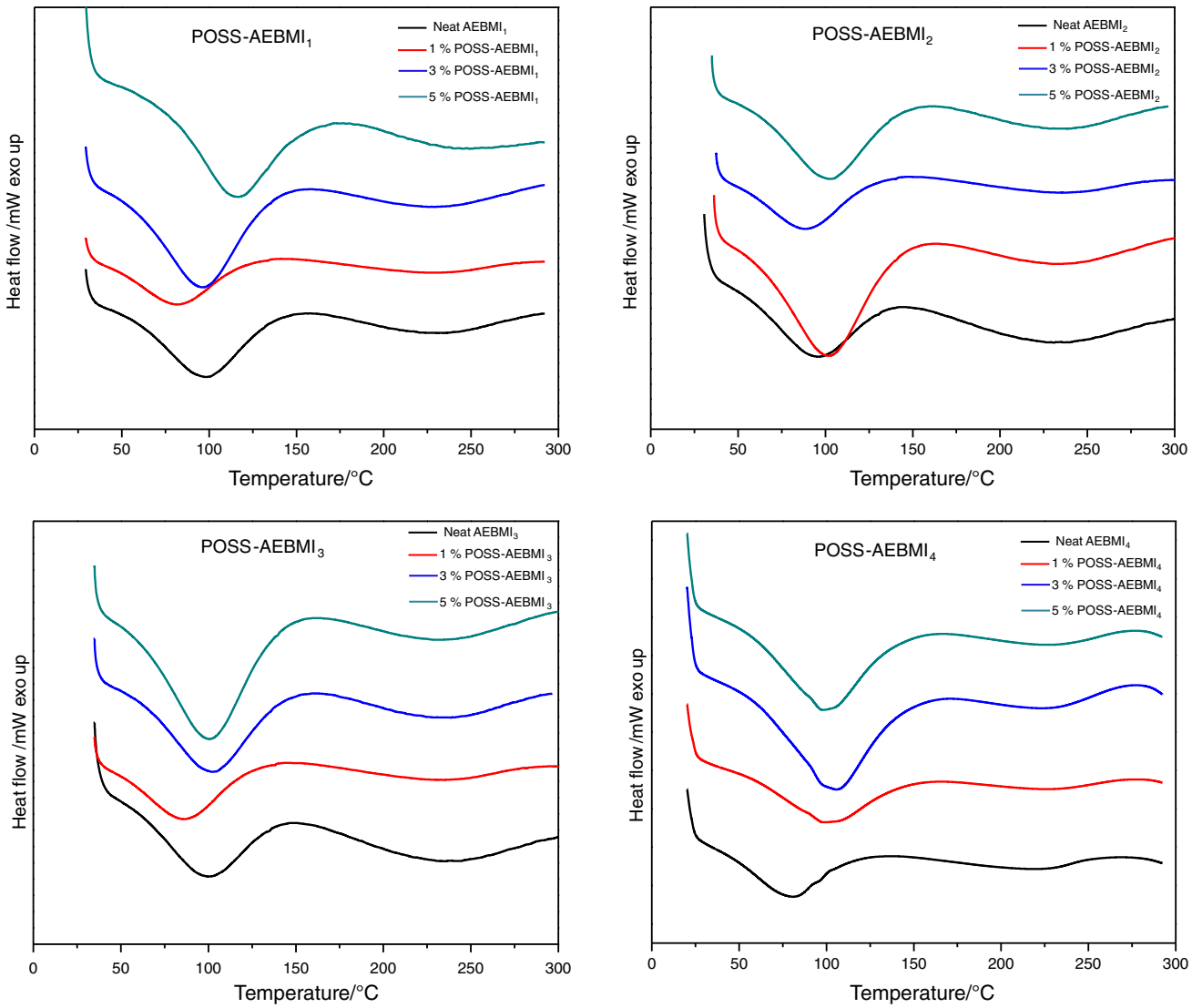

Fig. 11 DSC curve of neat AEBMI and POSS-AEBMI nanocomposites

dielectric behavior, as mentioned in our previous work, was observed for POSS nanocomposites [21–26].

It is commonly known that the signal propagation delay time of the integrated circuits is proportional to the square root of the dielectric constant of the hybrid nanocomposites, and therefore, the signal propagation is directly proportional to the dielectric constant and dielectric loss of the hybrid composites. Thus, the values of low dielectric constant and low dielectric loss increase the speed of signal transmission between the chips in the packaging materials [25]. Hence, the hybrid nanomaterials developed in the present work with good dielectric behavior may find better utility in microelectronic insulation applications.

XRD is used to characterize the organic–inorganic hybrid network structure of OAPS, AEBMI, and POSS-AEBMI nanocomposites, with respect to the changes in the value of 2θ using Bragg's law $2dsin\theta = n\lambda$, where θ is the (angle of diffraction) Bragg angle, λ is the wavelength used, and n is the order of the crystalline plane. The XRD patterns for the neat OAPS and OAPS-reinforced AEBMI systems are shown in Fig. 16. From Fig. 16, a strong peak at$2\theta = 7.7°$ (d-spacing 1.11 nm represents the inter cubic distance of OAPS) was observed. The diffraction pattern of OAPS-reinforced AEBMI system showed a broad amorphous peak at $2\theta = 18.31°$, which suggested that the OAPS molecules are completely dispersed in the AEBMI matrix systems. The XRD pattern of all the POSS-AEBMI nanocomposites is similar, and implies that OAPS is homogeneously dispersed in the AEBMI networks.

Figure 17 show the TEM micrographs of 5 mass% of POSS-reinforced AEBMI nanocomposites. It shows the

Table 1 Thermal and dielectric behavior of neat AEBMI and POSS-AEBMI

Systems	POSS mass/%	*Tg*/°C	TG				LOI/% 0.4 (σ) + 17.5 (N_2)	LOI/% 0.4 (σ) + 17.5 (Air)	Dielectric constant (ε') (1 MHz)
			10% mass loss /°C (N_2)	10% mass loss /°C (Air)	Char yield at 700/°C %(N_2)	Char yield at 700/°C %(Air)			
POSS-AEBMI$_1$	0	236.1	365	313	46.1	6.1	35.9	19.9	4.10
	1	238.2	300	320	49.0	7.1	37.1	20.3	3.84
	3	241.5	302	314	51.5	7.3	38.1	20.4	3.55
	5	245.2	352	319	52.7	8.2	38.6	20.8	3.19
POSS-AEBMI$_2$	0	234.2	330	314	41.1	4.1	33.9	19.1	3.93
	1	236.8	346	321	43.9	5.6	35.0	19.7	3.72
	3	241.2	358	320	46.7	7.1	36.2	20.3	3.35
	5	243.1	366	324	51.6	7.8	38.1	20.6	3.05
POSS-AEBMI$_3$	0	229.1	315	267	35.2	2.8	31.6	18.6	3.75
	1	232.5	331	297	39.0	3.2	33.1	18.8	3.36
	3	236.2	357	293	40.3	4.2	33.6	19.1	2.96
	5	240.1	380	314	46.6	5.6	36.1	19.7	2.70
POSS-AEBMI$_4$	0	223.7	310	305	32.4	2.3	30.5	18.4	3.43
	1	227.8	327	280	34.0	3.3	31.1	18.8	3.06
	3	230.9	365	289	35.2	4.5	31.6	19.3	2.66
	5	232.7	300	305	36.5	5.1	32.1	19.5	2.31

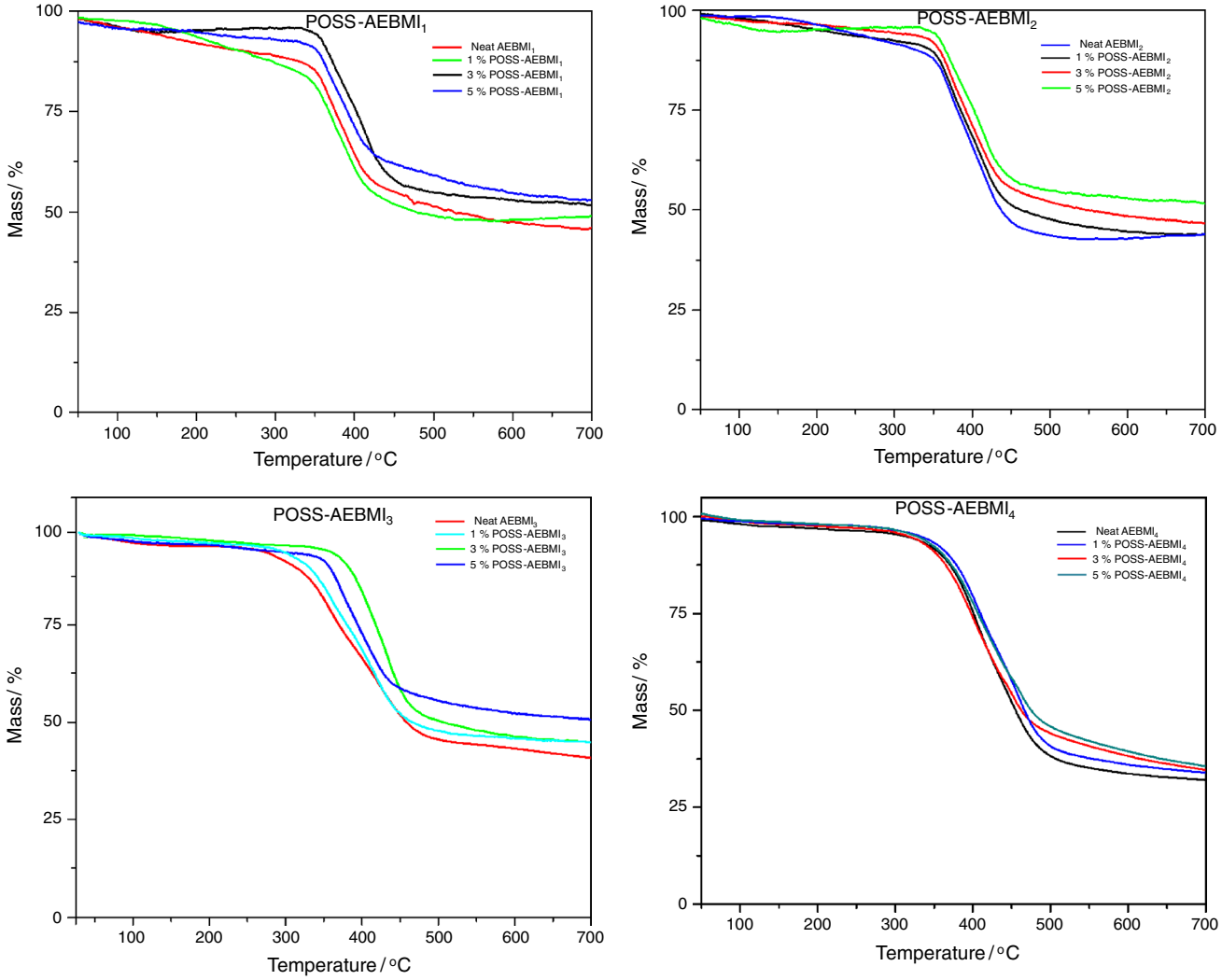

Fig. 12 TG curve of neat AEBMI and POSS-AEBMI nanocomposites in Nitrogen atmosphere

homogeneous morphology, and no localized domains were observed. Only a few darker points were observed at approximately about 30 nm in the AEBMI matrix, which represents the dispersion of the OAPS in the AEBMI matrix. This observation indicates that the nanocomposite is a material with a particle size of the dispersed phase having at least one dimension of <100 nm [37]. Thus, the POSS moieties are well dispersed at a nanometer scale in the AEBMI matrix to form a POSS-AEBMI network. These results reveal that the hybrid nanocomposites showed good interfacial interaction between POSS and AEBMI matrix. The nanometer level dispersion of POSS in the AEBMI matrix also indicates that there should be an influence on the other properties of the polymer.

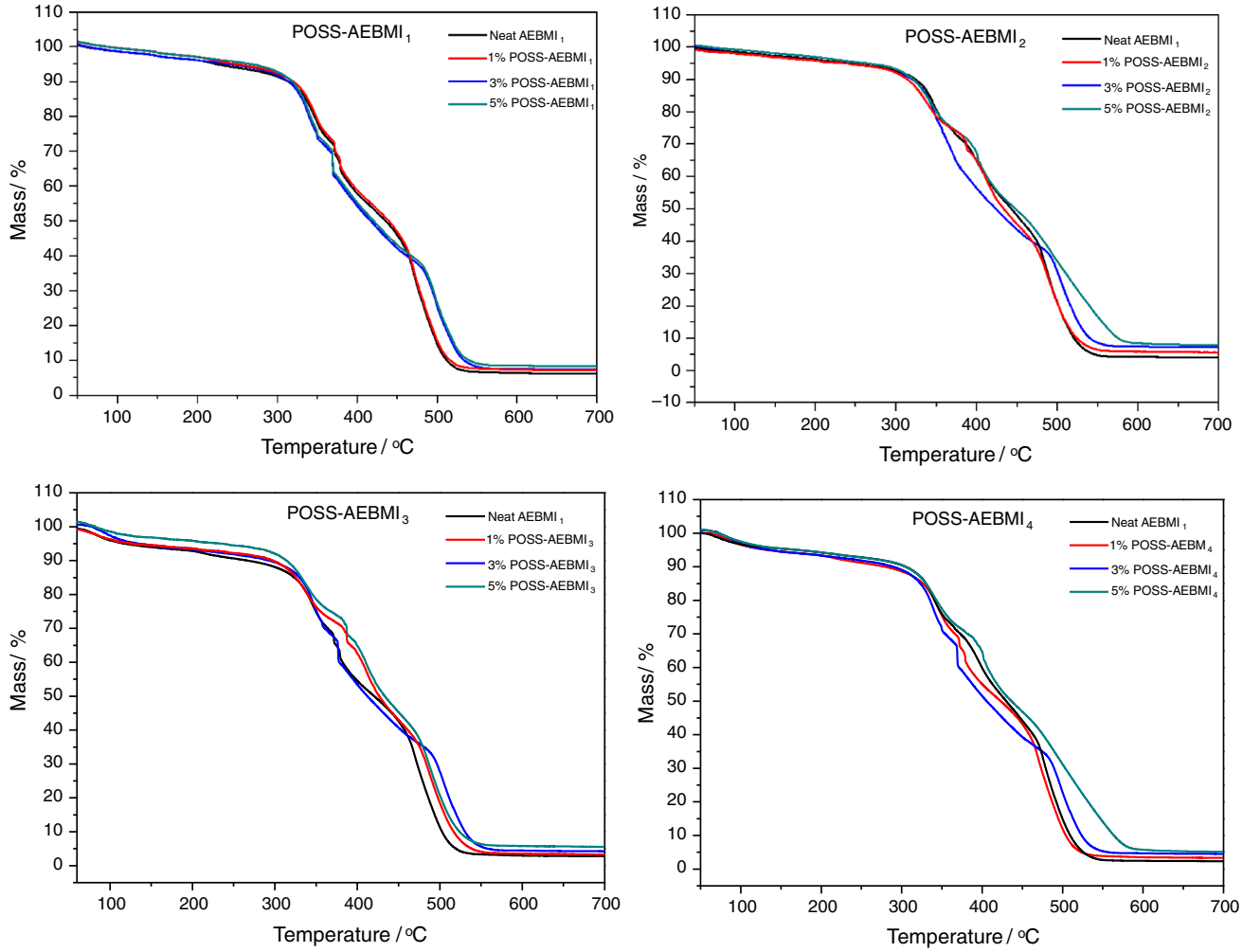

Fig. 13 TG curve of neat AEBMI and POSS-AEBMI nanocomposites in air atmosphere

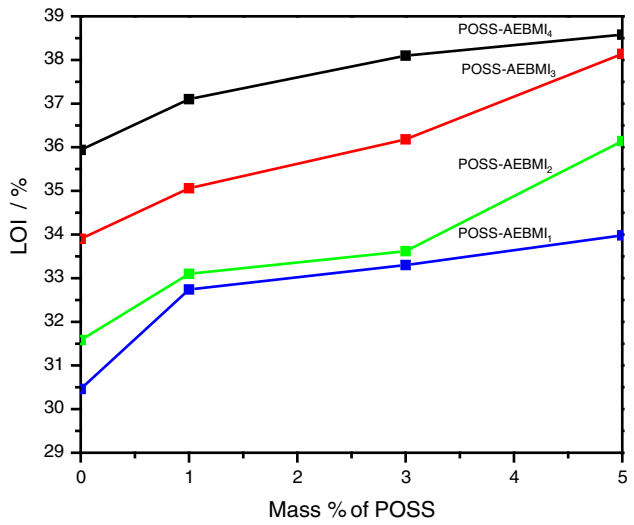

Fig. 14 LOI value of neat AEBMI and POSS-AEBMI nanocomposites

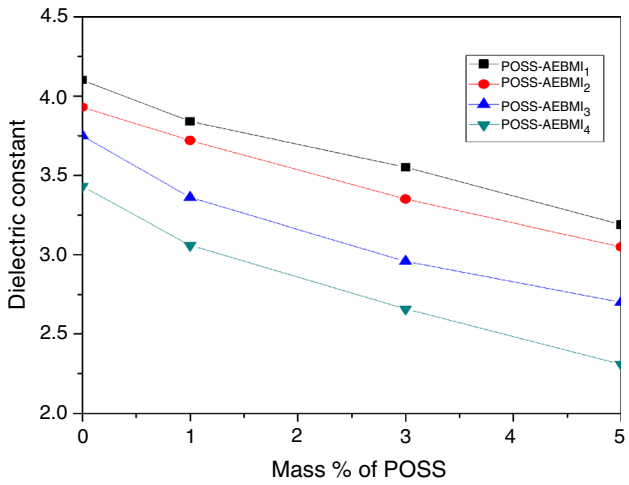

Fig. 15 Dielectric constant values of neat AEBMI and POSS-AEBMI nanocomposites

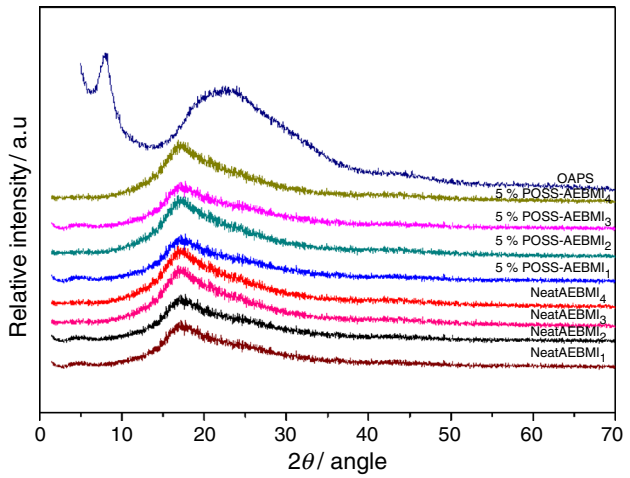

Fig. 16 XRD patterns of AEBMI and POSS-AEBMI nanocomposites

Conclusions

Four new types of POSS-incorporated linear aliphatic ether-linked aromatic bismaleimide-based POSS-AEBMI nanocomposites were developed and characterized. The linear aliphatic ether-linked aromatic BMI was synthesized, using the respective linear aliphatic ether-linked aromatic diamines and maleic anhydride. The OAPS-incorporated AEBMIs show higher values of *Tg*, better thermal stability, and low k dielectric properties than those of neat AEBMIs, and these hybrid materials are expected to find a wide range of applications in the field of aerospace and microelectronics, for better performance and longevity.

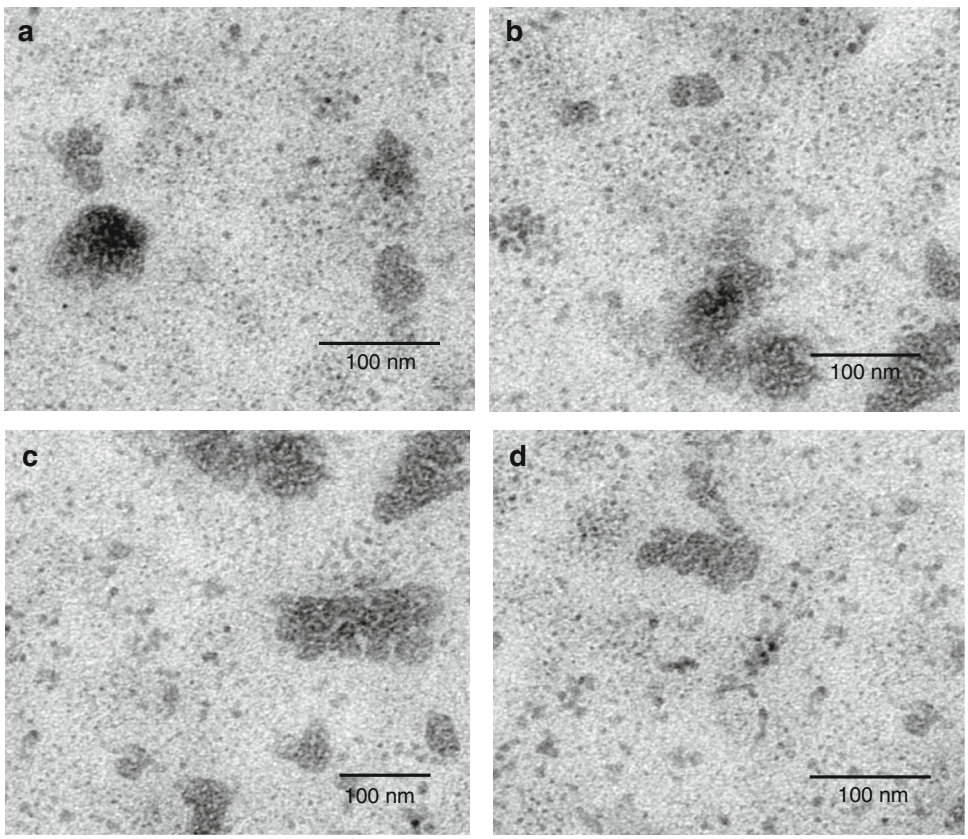

Fig. 17 TEM micrograph of **a**. 5 mass% POSS-AEBMI$_1$, **b**. 5 mass% POSS-AEBMI$_2$, **c**. 5 mass% POSS-AEBMI$_3$, and **d**. 5 mass% POSS-AEBMI$_4$

Acknowledgements The authors thank BRNS, G. No: 2012/37C/9/BRNS, Mumbai, Govt. of India., for the financial support, and also thank Dr. Manmohan Kumar, Senior Scientific Officer, BARC, Mumbai. Also author thank PSG College of Technology, Coimbatore for providing TEM facility.

References

1. Maclachlan MJ, Manners I, Ozin GA. New (inter) faces: polymers and inorganic materials. Adv Mater. 2000;12:675–81.
2. Chandross EA, Miller RD. Nanostructures: introduction. Chem Rev. 1999;99:1641–2.
3. Gomez-Romero P. Hybrid organic-inorganic materials—in search of synergic activity. Adv Mater. 2001;13:163–74.
4. Lee YJ, Kuo SW, Huang CF, Chang FC. Synthesis and characterization of polybenzoxazine networks nanocomposites containing multifunctional polyhedral oligomeric silsesquioxane (POSS). Polymer. 2006;47:4378–86.
5. Sanchez C, Belleville P, Popall M, Nicole L. Applications of advanced hybrid organic–inorganic nanomaterials: from laboratory to market. Chem Soc Rev. 2011;40:696–753.
6. Sanchez C, Shea KJ, Kitagawa S. Recent progress in hybrid materials science. Chem Soc Rev. 2011;40:471–2.
7. Fina A, Tabuani D, Frache A, Camino G. Polypropylene–polyhedral oligomeric silsesquioxanes (POSS) nanocomposites. Polymer. 2005;46:7855–66.
8. Ricco L, Russo S, Monticelli O, Bordo M, Bellucci F. ε-Caprolactam polymerization in presence of polyhedral oligomeric silsesquioxanes (POSS). Polymer. 2005;46:6810–9.
9. Kopesky ET, Haddad T, Mckinley GH, Cohen RE. Miscibility and viscoelastic properties of acrylic polyhedral oligomeric silsesquioxane–poly(methyl methacrylate) blends. Polymer. 2005;46:4743–52.
10. Zhang W, Müller AHE. Architecture, self-assembly and properties of well-defined hybrid polymers based on polyhedral oligomeric silsesquioxane (POSS). Prog Polym Sci. 2013;38:1121–62.
11. Laine RM. Nanobuilding blocks based on the $[OSiO1.5]_x$ ($x^\circ = {}^\circ 6$, 8, 10) octasilsesquioxanes. J Mater Chem. 2005;15:3725–44.
12. Liu HZ, Zheng SX, Nie KM. Morphology and thermomechanical properties of organiceinorganic hybrid composites involving epoxy resin and an incompletely condensed polyhedral oligomeric silsesquioxane. Macromolecules. 2005;38:5088–97.
13. Cordes DB, Lickiss PD, Rataboul F. Recent developments in the chemistry of cubic polyhedral oligosilsesquioxanes. Chem Rev. 2010;110:2081–173.
14. Kuo SW, Chang FC. POSS related polymer nanocomposites. Prog Polym Sci. 2011;36:1649–96.
15. Xu H, Kuo S, Lee J, Chang F. Preparations thermal properties, and tg increase mechanism of inorganic/organic hybrid polymers based on polyhedral oligomeric silsesquioxanes. Macromolecules. 2002;35:8788–93.
16. Leu C, Reddy GM, Wei K, Shu C. Synthesis and dielectric properties of polyimide-chain-end tethered polyhedral oligomeric silsesquioxane nanocomposites. Chem Mater. 2003;15:2261–5.
17. Wu S, Hayakawa T, Kikuchi R, Grunzinger SJ, Kakimoto M. Synthesis and characterization of semiaromatic polyimides containing poss in main chain derived from double-decker-shaped silsesquioxane. Macromolecules. 2007;40:5698–705.
18. Blanco I, Abate L, Bottino FA, Bottino P. Hepta isobutyl polyhedral oligomeric silsesquioxanes (hib-POSS). J Therm Anal Calorim. 2012;108:807–15.
19. Blanco I, Abate L, Bottino FA, Bottino P, Chiacchio MA. Thermal degradation of differently substituted cyclopentyl polyhedral oligomeric silsesquioxane (CP-POSS) nanoparticles. J Therm Anal Calorim. 2012;107:1083–91.
20. Blanco I, Abate L, Bottino FA. Variously substituted phenyl hepta cyclopentyl-polyhedral oligomeric silsesquioxane (ph, hcp-POSS)/polystyrene (PS) nanocomposites. J Therm Anal Calorim. 2013;112:421–8.
21. Devaraju S, Venkatesan MR, Alagar M. Studies on thermal and dielectric properties of ether linked cyclohexyl diamine (ELCD)-based polyimide POSS nanocomposites (POSS-PI). High Perform Polym. 2011;23:99–111.
22. Devaraju S, Vengatesan MR, Selvi M, Ashok Kumar A, Alagar M. Synthesis and characterization of bisphenol-A ether diamine based polyimide POSS nanocomposites for low K dielectric and flame-retardant applications. High Perform Polym. 2012;24:84–96.
23. Chandramohan A, Nagendiran S, Alagar M. Synthesis and characterization of polyhedral oligomeric silsesquioxane–siloxane modified polyimide hybrid nanocomposites. J Compos Mater. 2012;46:773–81.
24. Chandramohan A, Devaraju S, Vengatesan MR, Alagar M. Octakis(dimethylsiloxypropylglycidylether)silsesquioxane (OG-POSS) reinforced 1,1-bis(3-methyl-4-hydroxyphenyl)cyclohexane based polybenzoxazine nanocomposites. J Polym Res. 2012;19:9903.
25. Venkatesan MR, Devaraju S, Ashok Kumar A, Alagar M. Studies on thermal and dielectric properties of Octa (maleimido phenyl) silsesquioxane (OMPS)—polybenzoxazine (PBZ) hybrid nanocomposites. High Perform Polym. 2011;23:441–56.
26. Venkatesan MR, Devaraju S, Dinakaran K, Alagar M. Studies on thermal and dielectrical properties of organo clay and octakis (dimethylsiloxypropylglycidylether) silsesquioxane (OG-POSS) filled polybenzoxazine (PBZ) hybrid nanocomposites. Polym Compos. 2012;32:1701–11.
27. Jothibasu S, Premkumar S, Alagar M, Hamerton I. Synthesis and characterization of a POSS-maleimide precursor for hybrid nanocomposites. High Perform Polym. 2008;20:67–85.
28. Nagendiran S, Alagar M, Hamerton I. Octasilsesquioxane reinforced DGEBA and TGDDM epoxy nanocomposites: characterization of thermal, dielectric and morphological properties. Acta Mater. 2010;58:3345–56.
29. Liaw DJ, Liaw BY, Chen JJ. Synthesis and characterization of new soluble polyaspartimides derived from bis(3-ethyl-5-methyl-4-maleimidophenyl)methane and various diamines. Polymer. 2001;42:867–72.
30. Fan J, Hu X, Yue CY. Thermal degradation study of interpenetrating polymer network based on modified bismaleimide resin and cyanate ester. Polym Int. 2003;52:15–22.
31. Guo ZS, Du SY, Zhang BM, Wu ZJ. Modeling the curing kinetics for a modified bismaleimide resin using isothermal DSC. J Appl Polym Sci. 2004;9:3338–42.
32. Boey FYC, Song XL, Yue CY, Zhao Q. Modeling the curing kinetics for a modified bismaleimide resin. J Polym Sci, Part A: Polym Chem. 2000;38:907–13.
33. Sunitha M, Nair CPR, Krishnan K, Ninan KN. Kinetics of Alderene reaction of Tris (2-allylphenoxy) triphenoxycyclotriphosphazene and bismaleimides—a DSC study. Thermochim Acta. 2001;374:159–69.
34. Huang FW, Rong ZX, Shen XN. Organic/inorganic hybrid bismaleimide resin with octa(aminophenyl)silsesquioxane. Polym Eng Sci. 2008;48:1022–8.
35. Han YJ, Liao GX, Xu YJ, Yu GP, Jian XG. Cure kinetics, phase behaviors, and fracture properties of bismaleimide resin toughened by poly(phthalazinone ether ketone). Polym Eng Sci. 2009;49:2301–8.
36. Ashok Kumar A, Alagar M, Rao RMVGK. Preparation and Characterization of Siliconized Epoxy/Bismaleimide (*N*,*N*'-Bismaleimido-4,4′-diphenylmethane) Intercrosslinked Matrices for Engineering Applications. J Appl Polym Sci. 2001;81:38–46.
37. Komarneni S. Feature article. Nanocomposites. J Mater Chem. 1992;2:1219–30.